Earth Surface Processes and Landforms
Earth Surf. Process. Landforms **24**, 393–412 (1999)

NEAR-BED MASS FLUX PROFILES IN AEOLIAN SAND TRANSPORT: HIGH-RESOLUTION MEASUREMENTS IN A WIND TUNNEL

GRAEME R. BUTTERFIELD*
Department of Geography, Queen Mary and Westfield College, University of London, Mile End Road, London E1 4NS, UK.

Received 7 September 1998; Revised 28 October 1998; Accepted 30 October 1998

ABSTRACT

Vertical profiles of the streamwise mass flux of blown sand in the near-bed (< 17 mm) region are analysed from high-resolution measurements made using an optical sensor in a wind tunnel. This analysis is complemented by detailed measurements of mass flux and mean velocity profiles throughout the boundary layer depth (0·17 m) using passive, chambered sand traps of small dimensions and armoured thermal anemometers, respectively. The data permit a preliminary analysis of the relations between the observed forms of the profiles of near-bed fluid stress and horizontal mass flux within a carefully conditioned boundary layer.

Profiles of mass flux density are found to be characterized by three regions of differing gradient with transitions at about 2 mm and 19 mm above the bed. The exponential decay of mass flux with height is confirmed for elevations above 19 mm, and when plotted as a function of u_*^2/g (a parameter of mean vertical trajectory height in saltation), the gradient of mass flux in this region scales with the wake-corrected friction velocity (u_{*_w}), where $u_{*_w} > 0{\cdot}30$ m s^{-1}. A separate near-bed region of more intense transport below 19 mm is identified which carries 80 per cent of the total mass flux. This region is evident in some previous field and wind tunnel data but not in profiles simulated by numerical models. Ventilated passive sand traps underestimate mass flux in this region by 37 per cent. At slow or moderate wind speeds a third significant region below 2 mm is observed. These regions are likely to be related to grain populations in successive saltation, low-energy ejections and intermittent bed contact, respectively. Optical measurements reveal locally high grain concentrations at some elevations below 5 mm; these heights scale with transport rate, mass flux gradient and wind speed.

KEY WORDS: aeolian mass flux; mass flux profile; optical sensor; transport rates

INTRODUCTION

Vertical profiles of horizontal mass flux in aeolian transport, and their relations to wind modification, are significant for the reliable prediction of transport rate and for verification of existing numerical models of aeolian sand transport employing trajectory calculations (e.g. Ungar and Haff, 1987; Werner, 1990; Anderson and Haff, 1991; McEwan, 1991; McEwan and Willetts, 1991; Sørensen, 1991; Spies, 1996; Spies and McEwan, 1999a, 1999b). They may also be significant for the vertical intensity of aeolian abrasion (Anderson, 1986). However, field and laboratory measurements employing aeolian sand traps are usually made with insufficient resolution to detect accurately the vertical distribution of near-bed transport within the lowest 5–10 per cent of the moving grain cloud (see Rasmussen and Mikkelsen, 1998). Given the established non-linearity of the profile of mass flux at higher elevations within the saltation layer (e.g. Zingg, 1953; Williams, 1964; Butterfield, 1991; White and Mounla, 1991; Chen *et al.*, 1996) and the vigorous nature of observed transport close to the bed (see Rice *et al.*, 1995, 1996), this deficiency has significant implications for the reliable estimation of total aeolian sand transport by wind, and for experimental verification of the modelled interactions between mass flux and stress distributions in the near-bed flow region.

* Correspondence to: Dr G. R. Butterfield, Department of Geography, Queen Mary and Westfield College, University of London, Mile End Road, London E1 4NS, UK. Email: G.R.Butterfield@qmw.ac.uk
Contract/grant sponsor: Natural Environment Research Council; contract/grant number: GR3/8413

CCC 0197-9337/99/050393–20 $17.50

For moderate and high wind speeds, existing field and wind tunnel data (e.g. White, 1982; Nalpanis, 1985; Rasmussen *et al.*, 1985; Butterfield, 1991; White and Mounla, 1991; Chen *et al.*, 1996; Rasmussen and Sørensen, 1999) demonstrate an exponential dependence of horizontal mass flux ($q_{(z)}$) on height (z) above a mobile sand surface. This dependence is most appropriately expressed as:

$$q_{(z)} = \alpha \mathrm{e}^{-\mathrm{z}/\beta} \tag{1}$$

where α is the mass flux at the surface ($z = 0$) and β is a length scale that defines the characteristic height of the mass flux profile. As grain trajectory heights should scale approximately with u_*^2/g (Owen, 1964; Anderson and Haff, 1991), Nalpanis (1985) and Nalpanis *et al*. (1993) suggest that $\beta = u_*^2/\lambda g$, where u_* is friction velocity and λ is a parameter that may be constant for a single experiment. However, exponential relations of this kind are not well constrained by flow variables (White and Schultz, 1977; Nalpanis, 1985; Nalpanis *et al.*, 1993), commonly show large residuals at both the higher and near-bed elevations (e.g. Butterfield, 1991), become increasingly uncertain at wind speeds near threshold (e.g. White and Mounla, 1991; Rasmussen and Sørensen, 1999), and have parameters that cannot easily be determined in 'any *a priori* way' (Nalpanis, 1985, p. 62). Indeed White and Mounla (1991) suggest that both α and λ may not be constants but functions of u_*, surface roughness and the distributions of particle size, shape and density.

In contrast, Stout and Zobeck (1996) demonstrate from field measurements on a sandy loam that the profile of mass flux within the fully developed near-surface layer below 25 cm is well represented by a modified power-law function of the form:

$$\frac{q_{(z)}}{\alpha} = \left(1 + \frac{z}{\sigma}\right)^{-2} \tag{2}$$

(i.e. ${q_{(z)}}^{0{\cdot}5}$ is a linear function of $(1 + z/\sigma)$) where σ is a scale height. Similar relations are suggested by Zingg (1953) and are supported by Sterk and Raats (1996) for sand transport below 50 cm.

Further, many published field and laboratory data show a separate log-linear region of increased mass flux below 15–20 mm from the bed. This feature is apparent in field measurements by Jensen *et al*. (1984), Butterfield (1991), Greeley *et al*. (1996) and Rasmussen and Sørensen (1999), and in wind tunnel studies by Kawamura (1951), White and Mounla (1991) and Rasmussen and Mikkelsen (1998). These investigations have used sand traps of various designs including closed or ventilated 'passive' types and fully aspirated 'active' types (Nickling and McKenna Neuman, 1997). However, this feature is not evident in the detailed field measurements of Rasmussen *et al*. (1985), the wind tunnel data of Williams (1964), or in the mass flux profiles predicted by the numerical models of McEwan and Willetts (1991) and Anderson and Haff (1991). That this obvious discrepancy in published work has not drawn more attention is perhaps surprising.

Much of the uncertainty in the empirical relations between mass flux, height and wind velocity arises from the low spatial resolution and probable inaccuracy of previous measurements of the profiles of mass flux in the region less than about 20 mm from the bed. It is well documented from both empirical measurements and numerical modelling that the majority of aeolian transport over mobile beds occurs within a few centimetres of the surface (e.g. Bagnold, 1941; Anderson and Haff, 1988; Butterfield, 1991; McKenna Neuman and Nickling, 1994; Stout and Zobeck, 1996). Within this near-bed region, however, flows are most sensitive to distortion by intrusive sand traps (see Horikawa and Shen, 1960; Nickling and McKenna Neuman, 1997) or grain impact sensors (e.g. Gillette and Stockton, 1989; Stockton and Gillette, 1990; Spaan and van den Abeele, 1991), and vertically integrated mass flux is usually measured over only one or two elevations below 20 mm (e.g. Williams, 1964; Greeley *et al.*, 1996). The available empirical data are, therefore, generally of insufficient vertical resolution and accuracy to permit analysis of the distributions of mass flux close to the bed and their relations to observed profiles of fluid stress. In addition, analysis of the influence of wind velocity on mass flux gradient has been constrained to some extent by the use of u_* to characterize the effects of wind speed on grain trajectory heights. The determination of u_* from velocity profile data is often ambiguous (Gerety, 1985; McKenna Neuman and Maljaars, 1997), especially in small wind tunnels where grain-modified flows may envelop the constant-stress region (see Spies *et al.*, 1995). There is a need,

therefore, for non-intrusive, high-resolution measurements of the profiles of near-bed transport rate, including the effects of surface creep and the entire spectrum of grain trajectories arising from low- and high-energy reptation, as well as established saltation. Ideally, such measurements should be supported by rigorous analysis of the stress distribution within the forcing wind.

The aims of the research reported here are threefold. Firstly, to investigate the vertical distribution of horizontal mass flux within the region $0 < z < 17$ mm in a wind tunnel using a newly developed optical sensor to make non-intrusive measurements of sand transport at high spatial resolution (*c*. 19 μm). Secondly, to measure vertical profiles of horizontal mass flux throughout the thickness of the boundary layer using a finely segmented 'Aarhus' type passive sand trap to permit comparison with published data from other, larger vertical array traps and with data obtained using the optical sensor. Finally, to attempt to constrain the parameters of mass flux gradient and to explore the nature of the mutual dependency of near-bed vertical distributions of mass flux and fluid stress in the confined boundary layer of a wind tunnel.

EXPERIMENTAL METHODS AND INSTRUMENTATION

The wind tunnel facility

The experiments reported were performed in the boundary layer wind tunnel at Queen Mary and Westfield College, University of London (QMUL). The QMUL tunnel is of the blow-down type and has a working section 8·2 m long with cross-sectional dimensions 0·3 m × 0·3 m. For the first 1·3 m length of the working section, flow traverses one of six arrays of matching roughness elements and turbulence spires (Figure 1). These are scaled, using a modified form of the method of Irwin (1981), to give an effective flow roughness commensurate with a selected, nominal steady-state value of u_* during saltation. The sand bed extends 6·9 m downwind of the roughness array and can be varied in depth between single grain thickness and 6 cm by adjustment of the floor in the working section. An adjustable sand feed mechanism allows the upwind sand input to be matched to measured mean sand output from the working section exit. A microprocessor-controlled inverter is used to control the speed of the three-phase motor and hence to provide precise control of the apparent freestream flow velocities (u_∞) above the boundary layer in the working section. Full details of the wind tunnel dimensions and operation are given in Butterfield (1993, 1998).

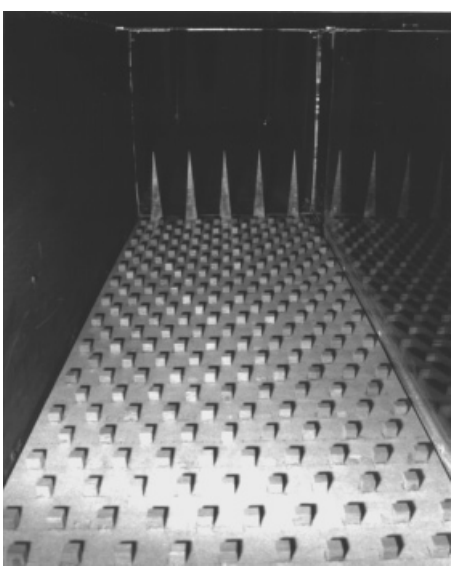

Figure 1. One of six spire-roughness arrays used to generate a thick boundary layer flow with nominal friction velocity (u_*) and effective roughness (z_o) matched to the values during saltation of sand 7·3 m downwind in the wind tunnel. Each array is 1·3 m long and 0·3 m wide. The dimensions of the spires and the spacing of the 9 mm cubic roughness elements both vary with nominal u_* value

In wind tunnels the free development of the boundary layer and the attainment of an equilibrium or steady-state saltation condition are constrained by the limited height (H) and length (x) of the working section. When tunnel dimensions are sufficient to avoid these effects, u_* (x) is approximately constant once any entrance effects have ceased and steady-state saltation is attained. White and Mounla (1991) and Owen and Gillette (1985) suggest that when the Froude number ($F = {u_1}^2/gH$, where u_1 is the freestream velocity upwind of the bed) is less than 10 or 20, respectively, saltation is unaffected by tunnel walls. In the QMUL tunnel, this Froude number is less than 10 for $u_1 \leq 5{\cdot}5$ m s^{-1}, and less than 20 for $u_1 \leq 7{\cdot}7$ m s^{-1}. Thus, in theory, at $u_1 > 7{\cdot}7$ m s^{-1} the tunnel does not meet either independence criterion for a freely developing boundary layer. However, the spires and roughness arrays in this case induce a prescribed boundary-layer thickness (δ) and u_* value at $x = 6h_s$ (where h_s is spire height) and measured variation in u_* for $x > 4$ m is slight. Constraints on saltation at $u_1 > 7{\cdot}7$ m s^{-1} are therefore likely to be less significant than implied by the theoretical independence criteria. In addition, the tunnel easily meets the most stringent minimum entrance length requirement ($x/\delta = 25$) suggested by White and Mounla (1991) for the establishment of equilibrium saltation.

Velocity measurement

Profiles of wind speed were obtained from point measurements of wind velocity made using an array of six, cross-calibrated, Dantec armoured hot-wire probes connected to six synchronized constant-temperature anemometers (see Butterfield, 1999). The probes are specially configured for measurements in thin boundary layers, and are mounted on traversing gear allowing them to be positioned vertically with an accuracy of $\pm 0{\cdot}5$ mm in the region $2 < z < 200$ mm above the bed. Velocities may be sampled at *c.* 10 Hz and automatically integrated over periods of 1 to 180 s.

Optical mass flux sensor

In this study, an optical mass flux sensor employing laser and charge-coupled device (CCD) technology was used to make measurements of the profile of mass flux within 17 mm above a mobile sand bed at high vertical resolution (19 μm). The physics, operation and calibration of the sensor are fully discussed in Butterfield (1999) and are outlined here.

The optical sensor detects differential light effects caused by grains traversing a laser sheet directed transverse to the flow. Collimated light from a 2mW, 670 nm laser is focused above the sand bed as a spanwise sheet (20 mm high) between two thin, aerodynamically shaped periscopes (5 mm $\times$ 68 mm) protruding through the sand bed (Figure 2). Airborne and surface particles move freely between the periscopes partially obscuring the light sheet.

Figure 3 shows a schematic of the sensor optics. The light sheet is focused on a line-scan camera mounted under one periscope (Figure 2). Elevation and separation of the periscopes are adjustable through 80 mm and 100 mm, respectively. Flow disturbance and interruption of bedform migration are minimal at separations of 50 mm or more (see Figure 2). The linear image sensor within the camera comprises 1024 low light receptive metal oxide semiconductor capacitors (referred to henceforth as 'pixels'), each 500 μm wide and centred 25 μm apart in an array 25·6 mm long. As the line beam is 20·0 mm high, the resolution of a near-bed mass flux gradient is of the order of 19 μm. Software in an interfaced desk-top computer controls the repetition frequency, refresh rate and integration time (adjustable from 1 ms to 20 ms for a periscope separation distance of 50 mm) and synchronizes the signals from the sensor with those from the anemometers. Maximum sampling frequency is conditioned by the sensor refresh and download rates. Sampling rates of between 4 Hz and 40 Hz are possible but 25 Hz is generally optimal.

As the sensor uses an undivided laser sheet, datum light signals for the unobstructed laser sheet must be determined for each pixel prior to a test run. Such signals remain stable for up to 240 s. During sand transport, in theory the amount of light integrated on the array of capacitors over a chosen sampling period is a function of the momentum (mass $\times$ velocity) of the grains traversing the laser sheet. Tests have shown that, although there is a significant dependence on light-scattering effects as well as light obscuration, single grains traversing the laser sheet leave a distinctive aggregate imprint in the light accumulated on the pixels of the array (Butterfield, 1999). Calibrations of total differential light aggregated on the entire array to mass flux

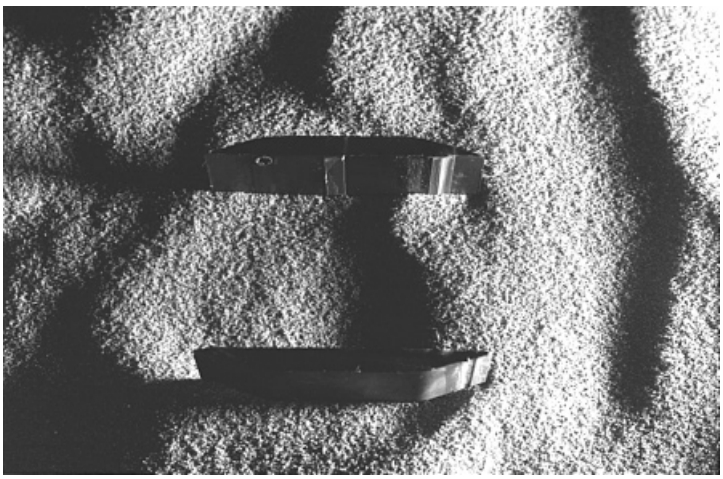

Figure 2. The laser/CCD optical sand transport sensor in the QMUL wind tunnel. The small dimensions and aerodynamic shape of the periscopes minimize flow disturbance and sand transport is unimpeded. Exposed sections of periscopes are 5 × 25 × 68 mm. The laser sheet is 20 mm high × 1·5 mm streamwise; its spanwise width at the setting shown is 50 mm but can be adjusted between 10 and 100 mm

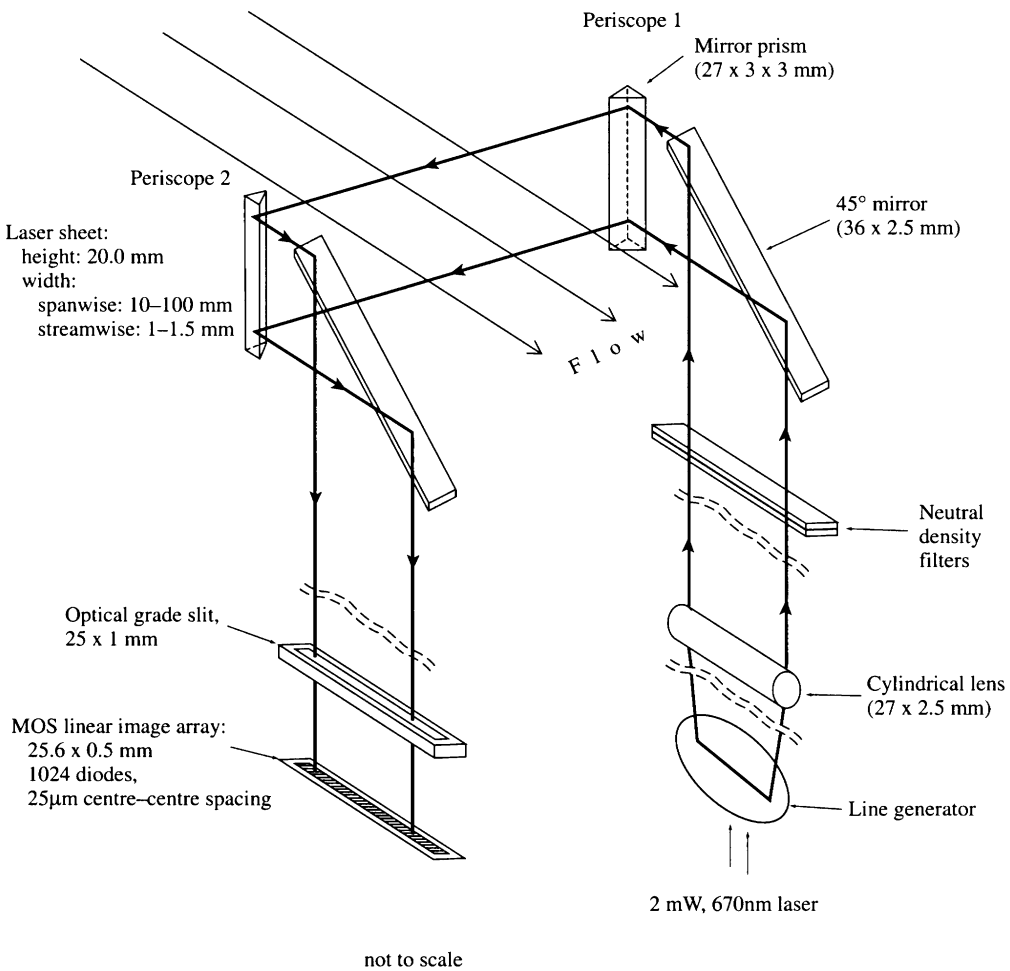

Figure 3. Optical components of the laser/CCD sand transport sensor (schematic and not to scale)

traversing the laser sheet have been derived for a range of grain velocities, total grain masses, integration times and spanwise dimensions of the laser sheet (Butterfield, 1999). These demonstrate that, within the range of calibrated flow velocities (3 to 8 m s^{-1}), the aggregated pixel signals register grain mass reliably and are relatively insensitive to grain velocity. Accordingly, appropriate calibrations of grain mass to values of the total integrated differential light per integration time may be applied with some confidence to experimental data from sand transport measurements. Extrapolation of such calibrations to data at pixel resolution is possible but results must be interpreted with caution.

Vertically segmented sand traps

To explore the form of the vertical distribution of mass flux obtained when conventional sand trapping techniques are applied at increased spatial resolution, and to complement the main data obtained using the optical sensor in the near-bed region $0 < z < 17$ mm, finely segmented, passive 'Aarhus' type sand traps were also used. These enabled mean transport rate profiles to be measured with a vertical resolution of 6·5 mm up to the maximum height reached by grain trajectories in the QMUL wind tunnel.

The traps are designed to be as small as possible, in keeping with the limited dimensions of the wind tunnel and to minimize flow distortion. They are constructed from polycarbonate, insulating 'twin-wall' (6 mm Lexan Thermoclear) manufactured in Denmark by Rias, and are 180 mm high, 150 mm in the streamwise dimension, and have 27 collection chambers. Wall thickness is just 300 μm, and the aperture of each chamber is 5 mm wide and 6·5 mm high. These dimensions permit a more detailed examination of the mass flux profile than has been achieved in most previous investigations. The traps are ventilated at the year by a 150 μm aperture nylon gauze.

Each trap may be suspended from the roof of the wind tunnel by rods attached by quick-release fittings. A collar around the rod allows a trap to be lowered rapidly to a predetermined level flush with the sand surface. The small capacity of the chambers means that sampling times must be restricted to periods of 10 to 30 s, depending on wind speed. At the end of the sampling period, the trap may be raised quickly to the roof of the tunnel. Arnold (1998) shows that in this position the traps have an insignificant effect on the boundary layer flow over the sand bed. Also, tests with empty traps held at the roof show that no sand grains are transported within the trap height (z = 120–300 mm) at wind speeds $u_\infty < 9{\cdot}0$ m s^{-1}.

Experimental procedures

A uniformly graded dune sand for which calibrations of the optical sensor were available was laid in the wind tunnel to a depth of 30 mm. After preparatory washing and screening, the sand had a mean grain size of 184 μm with 89·4 per cent by weight in the three 0·25 phi fractions spanning the size range 150–250 μm (Figure 4). The experiments reported here were conducted at six predetemined values of an apparent freestream velocity (u_∞) defined by the maximum velocity recorded between the thick boundary layer developed over the test bed and the thinner boundary layer at the tunnel roof, both measured at $x = 7{\cdot}3$ m. Over mobile beds of the test sand, airflows with u_∞ values of 6·34, 6·99, 7·74, 8·02 and 8·31 m s^{-1} were used, together with rates of upwind sand feeding matched to those at the exit of the working section. These velocities were selected to produce the corresponding nominal values of u_* generated by the matched sets of spires and roughness arrays. In addition, the mean velocity profile at a wind speed ($u_\infty = 6{\cdot}06$ m s^{-1}) just less than the threshold for transport was determined.

For each of the five mobile-bed experiments a standard procedure was followed. First, the bed and mass flux were allowed to adjust to the flow for 20 min. Mean velocity profiles during sand transport were then measured at a downwind distance $x = 7{\cdot}2$ m using the hot-wire array. Flow velocities sampled at 10 Hz were integrated over 10 s for each of 36 point measurements between $z = 4$ mm and 200 mm above the bed. Using the six-probe array the measurement of each mean velocity profile was completed in about 90 s.

Next, vertical profiles of horizontal mass flux were sampled at elevations below *c*. 17 mm using the optical mass flux sensor at $x = 7{\cdot}3$ m. To optimize the sensitivity of the sensor to the experimental conditions, a 40 ms repetition frequency (25 Hz sampling) and a periscope separation of 50 mm were used in all measurements. With velocity temporarily reduced to a sub-threshold value, the unobscured light integrated on each pixel

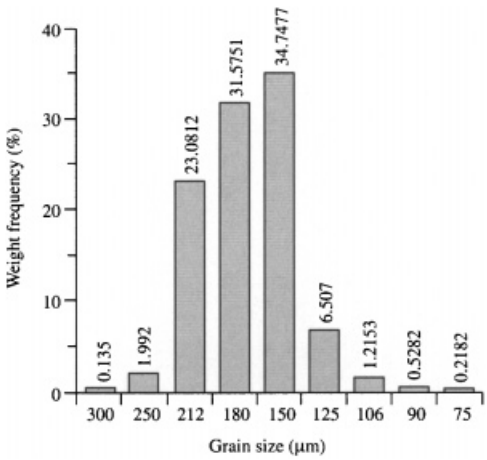

Figure 4. Grain size frequency distribution of the prepared dune sand used in the wind tunnel experiments. Mean size is 184 μm

(E_{oi}) of the sensor was first determined for 600 integrations each of 20 ms duration. Once the transport rate had restabilized at the required velocity for the experiment, mass flux was sampled 20 times using integrations of 20 ms duration to permit short-term profiles of mass flux to be determined. All measurements with the optical sensor were made at a standard position near the crest of a bed ripple. Because of differences in bed elevations at the times of measurement in the five experiments, the maximum detection height varied between 15 mm and 18 mm.

Finally, and immediately following the optical measurements, the mean mass flux profile at elevations < 180 mm was measured at $x = 7{\cdot}1$ m. Once sand transport had stabilized, an Aarhus trap was lowered rapidly to the bed so that it sampled the sand transport over a ripple crest. The trap remained in this position for exactly 30 s during which time small adjustments were made manually to the trap elevation to ensure contiguity with the crestal region of a ripple throughout the sampling period. The partially filled trap was then raised rapidly to the tunnel roof, removed through a roof door and an identical trap was fitted. This procedure was repeated between six and ten times, depending upon wind velocity. On each occasion the trap was lowered to sample at or near a ripple crest. The aggregated contents of each trap chamber were subsequently weighed to 0·01 mg using an analytical balance.

RESULTS AND DISCUSSION

Wind profile modification

The characteristics of the boundary layer flow at $x = 7{\cdot}3$ m for each of the six experiments are summarized in Table I, and Figure 5 shows the six mean velocity profiles plotted conventionally against logarithmic height. In all cases the introduction of spires and roughness arrays has increased the boundary layer thickness (δ) from 0·12 m to c. 0·17 m, where $u_{(\delta)}/u_\infty = 0{\cdot}99$. For the clean air case (Run F, $u_\infty = 6{\cdot}06$ m s^{-1}), the profile is almost perfectly log-linear ($r^2 = 0{\cdot}998$) with just a hint of convexity. Friction velocity was therefore determined for this profile using a form of the 'Law of the Wall';

$$u_{(z)} = \frac{u_*}{\kappa} \ln \frac{z}{z_o} \tag{3}$$

where κ is von Kármán's constant (0·41), and z_o is the roughness length. All profiles measured over mobile beds (Runs A–E), however, show the expected progressive departures from the clean air case (Run F) as u_∞ increases. Each consists of two log-linear segments consistently within the height ranges 0·05 to 0·17 m and 0·004 to 0·02 m, respectively, and separated by a transitional zone. A linear fit to all velocity values measured

Table I. Boundary layer flow characteristics at downwind distance x = 7·2 m in the wind tunnel

	Run A	B	C	D	E	F
Boundary layer flow						
u_∞ (m s^{-1})	6·34	6·99	7·74	8·02	8·31	6·06
δ (m)	0·17	0·17	0·17	0·17	0·17	0·17
u_{*_w} (m s^{-1})	0·27	0·34	0·37	0·40	0·44	0·25
u_* (m s^{-1})	-	-	-	-	-	0·34
Flow 0·05 m $< z < \delta$						
u_* (m s^{-1})	0·50	0·63	0·70	0·71	0·87	0·35
$z_o \times 10^3$ (m)	1·03	1·82	1·85	1·70	3·54	0·14
$C_o \times 10^2$	7·95	9·11	7·35	6·63	9·07	-
Flow 0·004 m $< z <$ 0·05 m						
u_* (m s^{-1})	0·25	0·32	0·33	0·40	0·38	0·33
$z_o \times 10^3$ (m)	0·02	0·11	0·06	0·15	0·14	0·14
$C_o \times 10^2$	0·80	1·84	1·13	1·86	1·88	-
Transport rate						
$Q_s \times 10^2$ (kg m^{-1} s^{-1})	0·808	1·414	1·756	2·205	3·127	nil

u_∞ is apparent freestream velocity; δ is boundary layer thickness; z is height above the bed; u_{*_w} is friction velocity calculated from the wake-corrected velocity profile; u_* is friction velocity calculated from the upper log-linear flow region; z_o is the effective roughness; $C_o = 2gz_o/u_*^2$; and Q_s is mass flux at $z < 13$ mm measured by the optical sensor

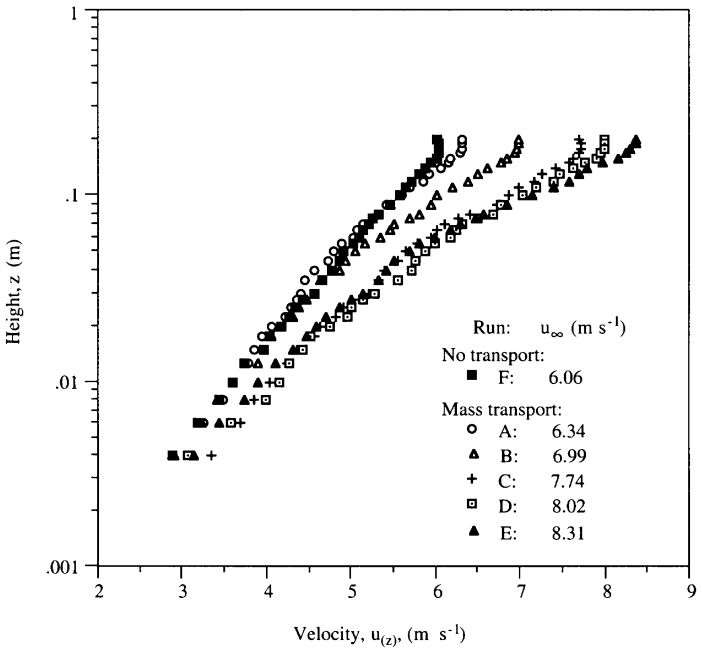

Figure 5. The six mean velocity profiles at distance x = 7·3 m downwind of entry plotted conventionally against logarithmic height. u_∞ is the apparent freestream velocity

at $z < \delta$ in such kinked velocity profiles is clearly inappropriate for the determination of friction velocity. However, if profiles of streamwise mass flux are to be related to fluid stress profiles and grain trajectory heights scaled by u_*^2/g, then the correct determination of friction velocity is not trivial.

For thick boundary layers, 'kinked' profiles of the type shown in Figure 5 are commonly interpreted as comprising a near-bed segment of lower gradient in which flow velocity is affected by grain-borne shear

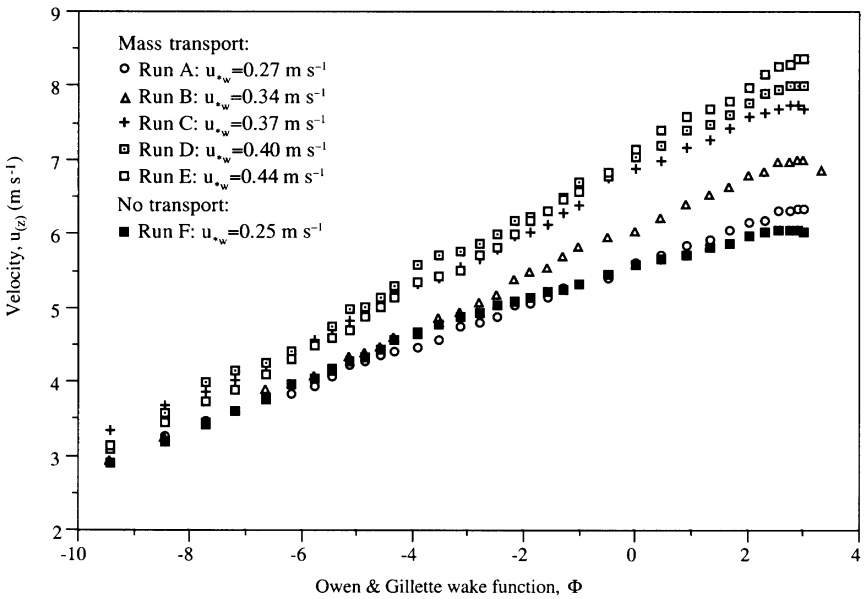

Figure 6. Velocity profiles plotted using Owen and Gillette's (1985) wake function (Equation 4). Values of friction velocity (u_{*w}) were calculated from these relationships

stress, and an upper segment of higher gradient and 'constant stress' from which u_* may be properly calculated using Equation 3 (Gerety, 1985; McEwan, 1993; McEwan and Willetts, 1993; McKenna Neuman and Nickling, 1994). The upward convexity of such velocity profiles is an inevitable consequence of the distributions of grain-borne shear stress and fluid shear stress in the grain layer (Owen, 1964; Anderson and Haff, 1991) and is widely observed in data from field and wind tunnel measurements (e.g. Gerety, 1985; White and Mounla, 1991), and in wind profiles calculated by numerical models (e.g. Anderson and Haff, 1991; McEwan and Willetts, 1991). For the present data, regression analysis shows the gradient of the upper segment (equivalent to u_*/κ assuming the 'Law of the Wall') increases markedly with u_∞ whilst that of the lower segment changes much less.

However, Spies *et al.* (1995) argue that when δ is less than *c.* 0·2 m, the constant-stress region (usually $< 0{\cdot}1\delta$) will be restricted to about 2–4 cm from the bed and may be subsumed within the height of a moving grain cloud. Thus they argue that in thin, confined boundary layers of small wind tunnels, flow in the upper segment represents a 'wake departure' occupying 80–90 per cent of the boundary layer thickness. If this is the case and, as in these experiments, the majority of velocity measurements are taken within this upper flow segment, then u_* should be calculated from Coles' (1956) 'Law of the Wake' applied to the entire profile using an appropriate wake correction. Janin and Cermak (1988) demonstrate that such wake-adjusted forms of the common logarithmic profile are applicable throughout the entire boundary layer, including that portion occupied by saltation.

Accordingly, Cole's (1956) wake function $w(z/\delta) = 1 - \cos(\pi z/\delta)$ was applied to all six profiles, and friction velocity (u_{*w}) was calculated from the 'wake-corrected' profiles using the methods of Owen and Gillette (1985) and White and Mounla (1991). Plotting velocity $u_{(z)}$ as a function of $\Phi(z/\delta)$, where:

$$\Phi = 1/\kappa[\ln(z/\delta) + 1/2\lambda(1 - \cos(\pi z/\delta))] \tag{4}$$

and $\lambda = 1{\cdot}2$ (equivalent to Cole's $\Pi = 0{\cdot}6$), the velocity profiles for the five runs over mobile beds show good linear relations and a consistent trend with increasing freestream velocity (Figure 6). This finding suggests that, in this wind tunnel, measured velocity profiles embracing a moving grain cloud exhibit a form of wake departure that is satisfactorily linearized by $\Phi(z/\delta)$.

Table I shows values of u_{*w} calculated from Figure 6, together with u_* values calculated for the log-linear velocity regions of each profile using Equation 3. Values of u_* for the upper flow region are much larger than expected from measurements in the field or in larger wind tunnels at comparable transport rates. Also, they do not scale well with mass flux (Q_S) measured by the optical sensor ($Q_S \propto u_*^{2.5}$), and are much larger than the corresponding design values predicted by the equations of Irwin (1981) for the boundary layers generated by the turbulence spires/roughness arrays. Further, Owen (1964) shows that effective bed roughness z_o during saltation varies with u_* according to the expression:

$$z_o = C_o u_*^{\,2}/2g \tag{5}$$

where C_o ranges between 0·01 and 0·06 depending on grain size and friction velocity (Rasmussen *et al.*, 1996). However, values of C_o calculated from upper flow data for Runs A–E (0·066 to 0·091) are larger than expected for a 184 μm sand and vary inconsistently with u_*. Collectively, these observations suggest that friction velocity is not correctly determined from upper flow segment velocity data from this wind tunnel facility.

If the velocity profile in the saltation layer is log-linear even close to the bed, as suggested by the results of Rasmussen *et al*. (1996), then data for elevations $4 < z < 20$ mm should yield appropriate values for u_*, z_o and C_o for grain-modified flows. Table I shows, however, that u_* values determined from this near-bed region vary inconsistently with both u_∞ and mass flux (e.g. $Q_S \propto u_*^{0.34}$), although for three profiles, C_o values are close to the expected tunnel value of 0·022. It is clear, therefore, that the near-bed log-linear velocity region does not correctly represent the effective shear stress during sand transport in this tunnel either.

In contrast, application of a wake-correction using Equation 4 satisfactorily linearizes the velocity profiles measured during saltation (Figure 6) and yields values of u_{*w} that are consistent with friction velocities recorded in larger wind tunnels and in the field, with expected threshold values, and with those prescribed by the spire design equations. Calculated values of u_{*w} also show the best relation to mass flux ($Q_S \propto u_{*w}^{2.75}$). In addition, although the velocity profile in clean air (Run F) is log-linear from $z = 0{\cdot}004$ m to $z = \delta = 0{\cdot}17$ m (Figure 5), u_* calculated from Equation 1 (0·34 m^{-1}) is too large for zero transport from a rippled bed of 184 μm sand. The value of z_o (0·0014 m) is of the expected order, however. Applying Equation 4 using the clean air value of the wake parameter $\Pi = 0{\cdot}55$ (Klebanoff, 1954; Janin and Cermak, 1988) yields $u_* = 0{\cdot}25$ m s^{-1} for this profile. This value is intuitively reasonable for a flow just less than threshold.

Thus there is strong evidence indicating that in these experiments using a wake correction with $\Pi = 0{\cdot}6$ yields friction velocities of the right order. Consequently the wake-corrected values of friction velocity (u_{*w}) are used in all analyses of the mass flux profile. The precision of the estimates of friction velocity may have been improved by application of a wake-correction procedure incorporating variation in Coles' wake parameter Π (e.g. White, 1991). Indeed Spies *et al*. (1995) show that Π is dependent on friction velocity. This analysis highlights, however, the uncertainties inherent in decoupling the effects of wind tunnel constraint from those due to modification of the stress profile by sand transport. The question remains, does the form of wind velocity profiles measured in a thin, confined boundary layer of a small wind tunnel contain information about the stress distribution that can be related meaningfully to the profile of horizontal mass flux?

Mass flux profiles at $z < 180$ mm: passive sand trap data

Raw weight data from each chamber of the segmented 'Aarhus' type traps were converted to horizontal mass flux ($q_{(z)}$) with dimensions kg m^{-2} s^{-1}. Dimensionless vertical profiles of horizontal mass flux for $z < 180$ mm at five wind speeds are shown in Figure 7. These show $q_{(z)}$ normalized on horizontal mass flux recorded by the near-bed trap chamber ($q_{(z1)}$) and plotted against z/H, where H is the height of the tunnel working section. For $u_{*w} > 0{\cdot}3$ m s^{-1}, all mass flux profiles show two regions of nearly perfect exponential decay of $q_{(z)}$ with height, each at a constant rate relative to the near-bed transport rate $q_{(z1)}$. Over elevations between 2 cm and 9 cm from the bed:

$$q_{(z)}/q_{(z1)} = 1 \cdot 29\ \mathrm{e}^{-28{\cdot}9z/H} \tag{6}$$

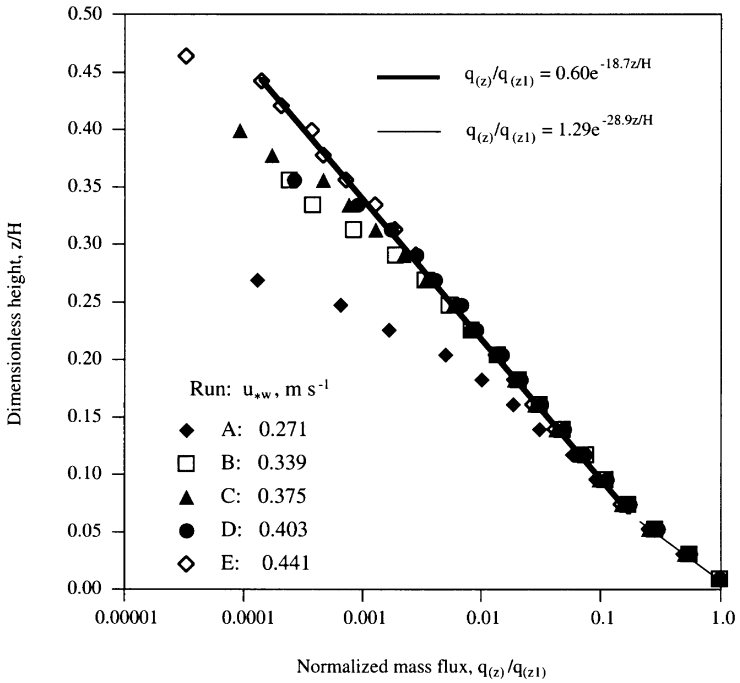

Figure 7. Dimensionless vertical profiles of horizontal mass flux ($q_{(z)}$) at $z < 180$ mm measured using the segmented sand trap and shown normalized on horizontal mass flux in the near-bed trap chamber [$q_{(z1)}$] for each of the five experiments. H is tunnel height (0·3 m)

whilst below 1·95 cm:

$$q_{(z)}/q_{(z1)} = 0 \cdot 60 \ \mathrm{e}^{-18 \cdot 7z/H} \tag{7}$$

For the friction velocity just exceeding threshold (Run A), however, the upper region of linear decay is less extensive and the mass flux profile appears to be in transition to the stable gradient form evident for faster wind speeds.

The vertical extent of the upper region of exponential decay increases with wind speed, but at the higher elevations of all profiles, measured fluxes are less than those predicted by the exponential decay function. This is attributable to a number of factors. Firstly, it is clear from consideration of energy conservation that there must exist a maximum saltation height for each grain size and wind speed. Thus, for a given wind speed, the grain size variation within the moving grain population will cause deviations from the exponential profile at the upper elevations, whilst increasing wind speed will cause the region of deviation to increase in elevation. Secondly, increasingly large percentage losses were incurred during the emptying and weighing of the small quantities of sand captured by the highest chambers. Finally, it is likely that the relative efficiency of the traps in capturing fine fractions declines at higher elevations and in faster flows. Therefore, the data scatter evident at the highest elevations is partly an artefact of the measurement procedures. It is clear, however, that for moderate or fast velocities, $q_{(z)}/q_{(z1)}$ is a constant negative exponential function of relative elevation above the bed within two separate flow regions, independent of wind speed.

To analyse the effects of wind speed on the mass flux gradients at $z > 20$ mm, transport rates were plotted following Equation 1 and using the vertical height scale ${u_*}_w^2/g$. Example plots for four experiments are shown in Figure 8. For all profiles, the data from the central trap chambers show excellent log-linear trends ($r^2 > 0{\cdot}99$) from which the profile parameters α and λ can be unambiguously determined. Again, for all but the slowest wind speed, transport rates measured by the lowest chambers ($z < 19{\cdot}5$ mm) show significant departures towards larger flux rates. In contrast to the results of White and Mounla (1991), values of α (Table II) for all but the near-threshold flow (Run A) are almost constant with wind speed, and λ increases linearly

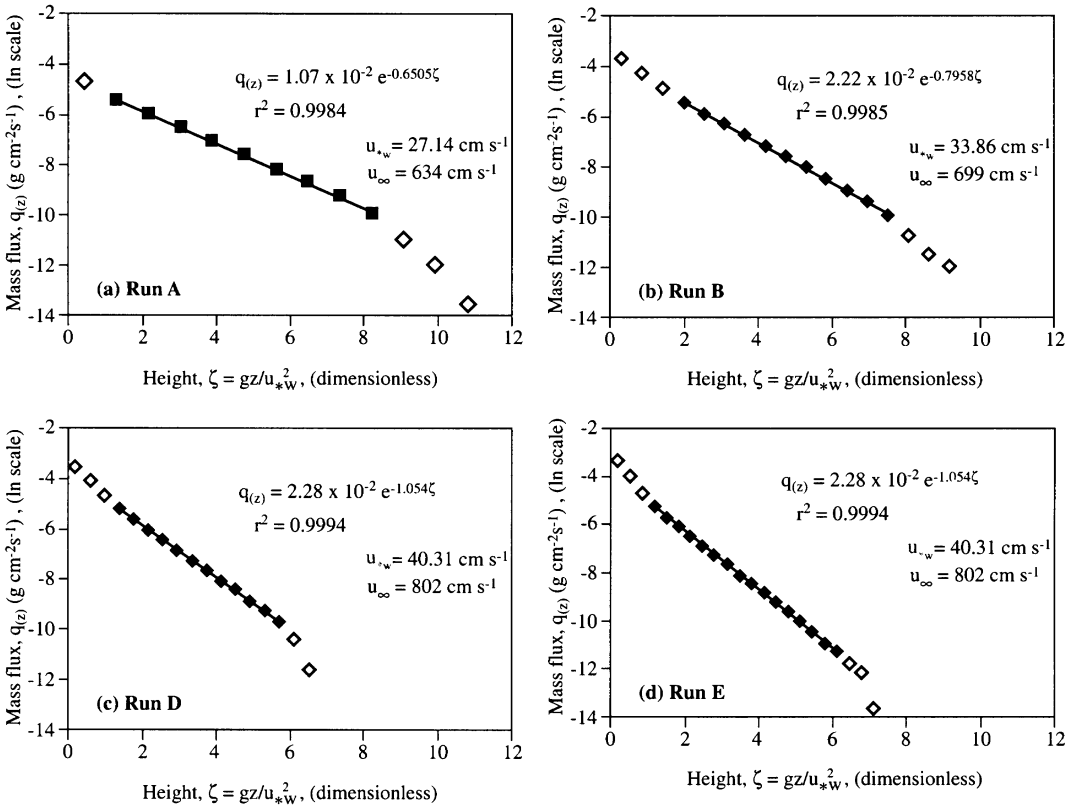

Figure 8. Mass flux ($q_{(z)}$) profiles for sand trap data plotted as a function of the dimensionless height scale $gz/u_{*_w}^2$

Table II. Parameters of mass flux profiles at z < 180 mm measured in the wind tunnel by passive Aarhus sand trap at downwind distance $x = 7{\cdot}1$ m

	Run A	B	C	D	E
$Q_t \times 10^2$ (kg m^{-1} s^{-1})*	0·651	1·098	1·359	1·674	2·216
Upper zone ($z > 19{\cdot}5$ mm)					
λ parameter (Eqn. 1)	−0·6505	−0·7958	−0·9644	−1·0540	−1·2197
α parameter (Eqn. 1)	0·0107	0·0222	0·0229	0·0228	0·0228
Lower zone ($z < 19{\cdot}5$ mm)					
λ parameter (Eqn. 1)	−0·8185	−1·1208	−1·5041	−1·5161	−2·6483
α parameter (Eqn. 1)	0·0127	0·0271	0·0415	0·0416	0·0517
% mass flux below 6·5 mm (0·04δ)	46·16	42·81	45·33	41·93	44·70
% mass flux below 13·0 mm (0·08δ)	68·88	66·60	68·28	65·79	68·55
% mass flux below 19·5 mm (0·12δ)	81·96	78·90	79·83	78·54	80·20

* Q_t is mass flux at $z < 13$ mm measured by segmented Aarhus sand traps.

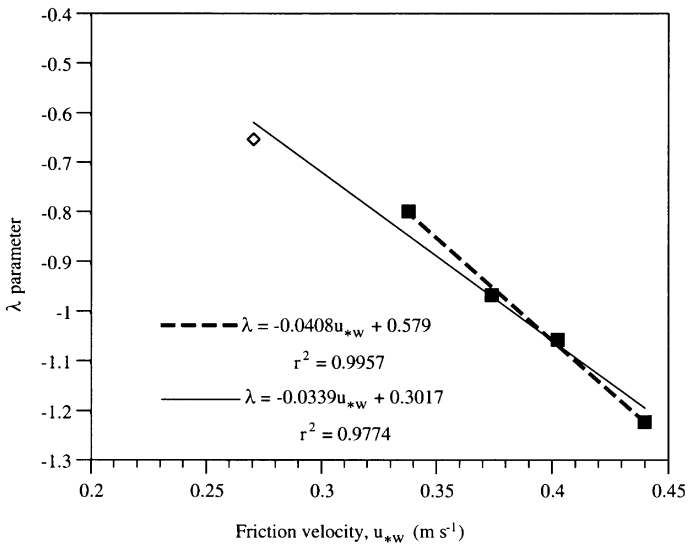

Figure 9. Relation between the λ parameter of mass flux gradient (Equation 1) and friction velocity (u_{*_w}) for sand trap data

with friction velocity (u_{*_w}) calculated from wake-corrected velocity profiles (Figure 9). Nalpanis *et al*. (1993) find that the coefficient λ is 0·9 and 1·2 for friction speeds of 0·28 and 0·35 m s^{-1}, respectively, in a wind tunnel. For the profiles measured by Rasmussen *et al*. (1985) on a beach these authors calculate that $\lambda = 0{\cdot}18$ for $u_* = 0{\cdot}63$ m s^{-1}.

Interpretation of λ depends on the assumption intrinsic to Equation 1 that the trajectory heights (h) of saltating grains scale with the vertical component of their ejection velocity (V_{ze}) from the bed. The detailed observations of grain impacts made by Rice *et al*. (1995, 1996) show that under the influence of gravity alone grains rise to a height $V_{ze}^2/2g$. Owen (1964) assumed that $V_{ze} = u_*$ and reasoned that $h \approx 0{\cdot}8u_*^2/g$. However, the results of White and Schultz (1977), Araoko and Maeno (1981) and Willetts and Rice (1985) demonstrate that V_{ze} is not well constrained by u_*. Nalpanis *et al*. (1993) find that, on average, $V_{ze} = 2u_*$ with a standard deviation of about 1·0 u_* and that $h/(u_*^2/g)$ lies between 1·4 and 1·6. Some of this variability may be due to imprecise determinations of u_*. Further, Sørensen (1985) shows that V_{ze} is strongly dependent upon grain size and decreases by a factor of 2 as grain size increases from 150 to 300 μm. Rice *et al*. (1985, 1995) demonstrate that with increasing particle size, ejection angle decreases and both the horizontal (V_{xe}) and vertical (V_{ze}) components of ejection velocity decrease. Williams (1964) found that the exponent in the mass concentration decay function $q_{(z)} = q_o e^{-bz}$ was affected markedly by grain shape, much less so by wind strength and the distribution of surface grain sizes, and not at all by friction velocity.

The height of grain trajectories will thus depend on particle size, shape and vertical ejection velocity. Hence for a single sand with given textural characteristics, values of α and λ are likely to be unique. Also, to compare gradients of mass flux measured over different sands $V_{ze}^2/2g$ would be a more appropriate height scale than u_*^2/g as it represents the vertical kinetic energy per unit weight of an ejected grain (Nalpanis *et al*., 1993), and in any case the relation between V_{ze} and u_* is uncertain. Unfortunately, for a given sand V_{ze} is not easily measurable. However, for the compact shapes of the single test sand used in the present experiments, λ is apparently well constrained by the friction velocity (u_{*w}) of moderate or fast winds.

All results from the trap measurements confirm previous observations that the vertical distribution of mass flux density does not follow a single log-linear curve. Below 19·5 mm (equivalent to 0·12δ or 0·065H) a region of intense mass flux with lower gradient accounts for about 80 per cent of the transport at all wind speeds, with 44 per cent occurring below 6·5 mm (0·04δ or 0·022H) (see Table II). However, the precise form of the distribution of transport within this region cannot be determined with certainty from the trap data and visual observations suggest that the rates in this region may be underestimated.

Although of extremely small dimensions, the Aarhus trap used in this investigation is relatively primitive. As the chambers are not fully aspirated, and the design gives no venturi effect, flow stagnation causes some scouring around the trap even during sample periods of less than 30 s. This is usual in non-isokinetic sand traps (Jones and Willetts, 1979; Shao *et al.*, 1993; Nickling and McKenna Neuman, 1997; Rasmussen and Mikkelsen, 1998) and probably leads to underestimation of transport rates at all elevations at low u_* but more so in the lowest chamber. Overfilling of this chamber may also lead to reduced ventilation and capture efficiency in vigorous transport conditions or in overlong sampling periods. The uniformity of the two observed gradients of $q_{(z)}/q_{(z1)}$ with wind speed suggests, however, that the trapping efficiency of each chamber is constant for the wind speeds used.

Plotting sand transport measured by the Aarhus traps (Q_t) for $z < 13$ mm against that measured by the independently calibrated optical sensor (Q_s) below the same height gives the relation $Q_t = 0{\cdot}63\ Q_s + 1{\cdot}1 \times 10^{-3}$. This indicates that the small Aarhus traps underestimate transport in this near-bed region by 37 per cent. This error is close to that recently documented by Rasmussen and Mikkelsen (1998) for traps of similar design. The distribution of this underestimation is unknown, but it is likely that a significant part of it arises from poor sampling of sand movements on and adjacent to the bed. Rasmussen and Mikkelsen (1998) find that trap efficiency approaches unity at a height of just 15 mm above the bed, so that it is likely that the mass flux profiles shown in Figure 8 are correct at elevations between 19 mm and 90 mm. The consistency of mass flux profile data and the robust relation between λ and friction velocity within these elevations in the present study reinforce this conclusion.

The trap data have confirmed the existence of a separate, dominant near-bed layer of enhanced mass flux below about 19 mm. It may be speculated that this is due to a population of ejecta resulting from grain impacts. Such populations are known to have markedly different distributions of V_{ze} (and hence average trajectory heights) from the grain populations experiencing successive saltation at higher elevations (Willetts and Rice, 1985, 1986; Rice *et al.*, 1995). The evidence from the three lowest chambers of the trap is insufficient to characterize accurately the gradients of the mass flux profile in this region, but further insight comes from the data obtained from the optical sensor.

Mass flux profiles at $z < 17$ mm: optical sensor data

Using the mean incident light (E_i) on each pixel per 20 ms integration period, the differential light effect recorded by each pixel of the optical mass flux sensor during transport events was calculated for each integration period as $\Delta(I_i) = (Eo_i - E_i)$. The average value of $\Delta(I_i)$ was then calculated over the 20 integrations in each run and the sensor calibration appropriate to the wind speed was applied to derive mass flux ($q_{(z)}$) in units g cm^{-2} s^{-1} through the *c.* 19 μm pixel elevation range. Values of mass flux derived in this way reveal transport rate profiles which are almost identical to the profiles of raw $\Delta(I_i)$ values and, being dimensionally consistent with other transport rate data, allow valid comparisons to be made with mass flux gradients determined from trap data. The absolute values of mass flux at pixel resolution must, however, be interpreted with considerable caution.

Raw values of Eo_i are small and constant for all pixels below the sand surface, but increase rapidly over a transitional zone of approximately 20 pixels to attain the sharply banded range typical of the large magnitude unobstructed light values above the surface. Bed elevation ($z = 0$) with no sand transport was defined by the lowest pixel registering a value equivalent to $-1{\cdot}0$ s.d. from the mean of the unobstructed Eo_i values well above the bed. To account for changes occurring between readings taken with and without sand transport, $z = 0$ was identified in profiles of $\Delta(I_i)$ values by the pixel at the corresponding position in the transition zone.

Figure 10 shows the vertical distributions of horizontal mass flux within approximately 17 mm of the sand bed for the four fastest wind speeds, plotted conventionally to highlight their form and structure. Vertical resolution is approximately 19 μm. The vertical extent of each profile varies slightly due to the differing exposure of the laser sheet for each run. For $u_\infty < 8{\cdot}0$ m s^{-1} the region below 2 mm from the bed is characterized by intense transport and a steep mass flux gradient; above about 6 mm, transport rate is much reduced and the gradient is more uniform. As u_∞ increases from 6·99 to 7·74 m s^{-1}, transport below 2 mm is little changed, but increased transport occurs at heights from 2 to 12 mm. This most probably reflects increasing numbers of higher grain trajectories and more energetic impact ejecta. At $u_\infty = 8{\cdot}11$ m s^{-1} (Figure

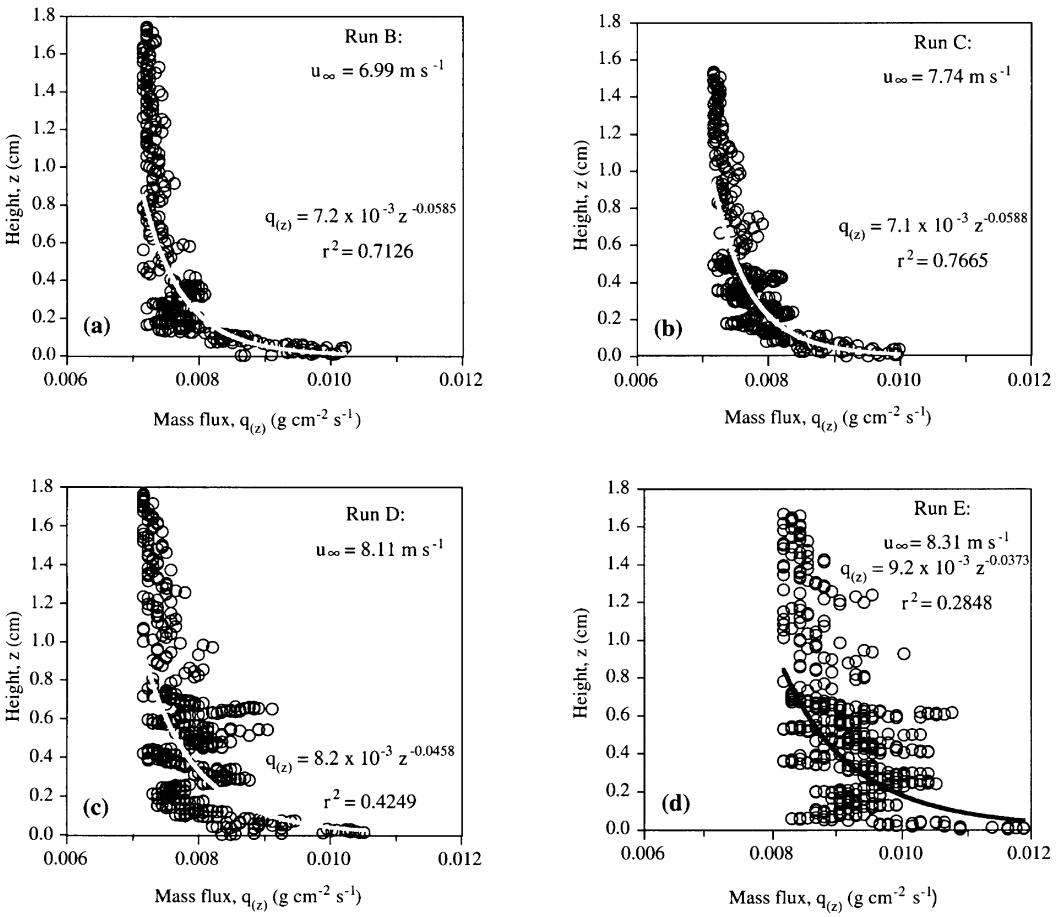

Figure 10. Vertical profiles of horizontal mass flux ($q_{(z)}$) within *c*. 17 mm of the sand bed measured by the optical sensor for the four fastest wind speeds. Vertical resolution is approximately 19 μm

10c) the profile shows increased variability at heights above 2 mm and a general displacement to increased rates at all elevations. At the fastest wind speed (Figure 10d), the profile of mass flux becomes less structured, has a steeper gradient, and the orderly pattern of transport below 2 mm is lost as more transport occurs in saltation trajectories further from the bed.

At all wind speeds the vertical profiles of mass flux show notable patterns of transport concentration that clearly show some velocity dependence (see Figure 10). These are not consistent with pixel number and are, therefore, not artefacts of the sensor itself. At the slowest velocity much of the transport is concentrated at a height of about 2 mm; at $u_\infty = 7{\cdot}74$ m s^{-1} enhanced transport occurs at elevations of 2·5 and 4·0 mm, and at $u_\infty = 8{\cdot}11$ m s^{-1} at 3·0 and 5·5 mm. At the fastest velocity the vertical pattern of transport becomes more chaotic but some preferred transport elevations are still discernible. These structural features in the data most likely reflect the vertical consistency of dominant grain trajectories in successive saltation in near-steady-state transport, and their vertical displacements in response to changing patterns of grain activity with increased wind speed.

Results from curve-fitting to mass flux data for $z < 15$ mm are given in Table III. Fitting exponential functions to all these data generally gives a poor fit with r^2 values decreasing in response to the increased scatter in the data for fast wind speeds (see Figure 10). However, for the three profiles at the slowest velocities, power functions of the form $q(z) = \gamma z^{-\psi}$ give high r^2 values significant at $p = 0{\cdot}01$. Plotting the data following Equation 1 against the vertical height scale u_*^2/g (Figure 11) suggests that the mass flux profiles below 15 mm may be interpreted as comprising two distinct but overlapping log-linear transport

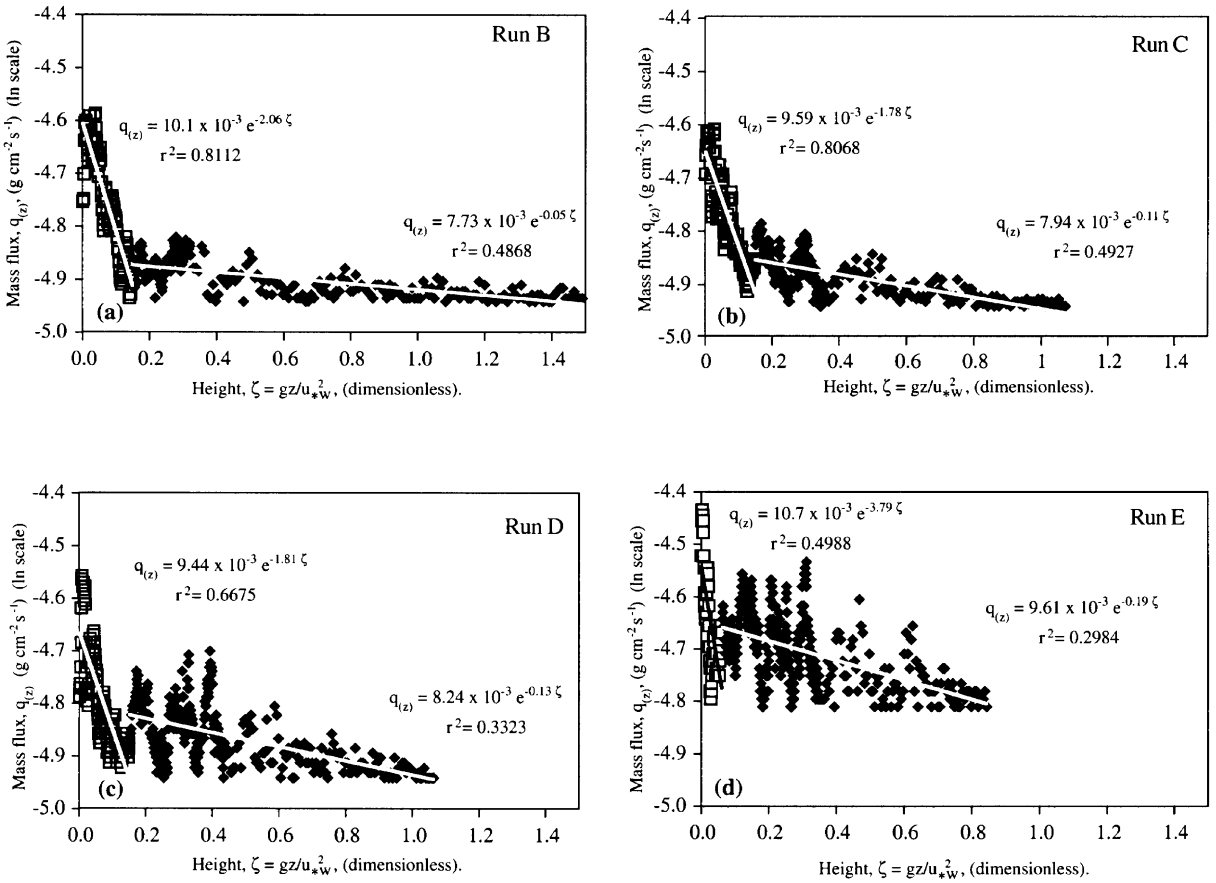

Figure 11. Near-bed profiles of horizontal mass flux ($q_{(z)}$) within *c*. 17 mm of the sand bed measured by the optical sensor and plotted as a function of the dimensionless height scale $gz/u_{*w}{}^2$

zones, each with velocity-dependent characteristics. As u_∞ increments from 6·34 to 8·11 m s^{-1}, the proportion of sand transported in the lowest zone decreases from 37 to 29 per cent, the height of the zone increases from 1·5 to 2·5 mm, and the slope parameter λ decreases (Table III). For the fastest velocity case (Figure 11 d), this transport population degenerates and the log-linear fit is much less convincing. Though the goodness-of-fit is poorer, λ values for the higher zone between *c*.2 and 15 mm (Zone 2, Table III) increase linearly with wind speed just as those for the lower log-linear zone detected by the sand trap. However, values of λ determined from the optical sensor are considerably smaller (cf. Tables II and III) reflecting the greatly increased detection of grain motion within 10–15 mm of the bed. These results clearly show that trap data greatly underestimate both the magnitude of mass flux below 15 mm and its profile gradient.

CONCLUSIONS

A number of significant conclusions can be drawn from the analysis presented above.

- Near-bed profiles of horizontal mass flux in a wind tunnel are characterized by three regions with transitions at approximately 2 mm and 19 mm above the bed, irrespective of wind speed.
- Above *c*.19 mm from the bed an exponential decay in mass flux is confirmed by detailed measurements with a passive trap of small dimensions. This region makes a minor contribution to total mass flux

Table III. Parameters of mass flux profiles at z < 15 mm measured in the wind tunnel by the optical mass flux sensor at downwind distance $x = 7{\cdot}3$ m

	Run				
	A	B	C	D	E
$Q_s \times 10^2$ (kg m^{-1} s^{-1})*	0·808	1·414	1·756	2·205	3·127
Exponential function, $q_{(z)} = ae^{-bz}$					
b	−0·1103	−0·1045	−0·1264	−0·0937	−0·0938
r^2	0·5126	0·3893	0·4645	0·3043	0·2748
Power function, $q_{(z)} = \gamma z^{-\psi}$					
ψ	−0·0572	−0·0585	−0·0588	−0·0458	−0·0373
r^2	0·7461	0·7126	0·7665	0·4249	0·2848
Exponential function, $q_{(z)} = \alpha e^{-(\lambda gz/u_{*w}2)}$					
Height of flux zone 1 (mm)	1·524	1·758	2·100	2·500	1·230
Zone 1: proportion of Q_s	0·3750	0·3220	0·3250	0·2918	0·1493
λ	−2·5211	−2·0566	−1·7724	−1·8122	−3·7936
r^2	0·8256	0·8112	0·8068	0·6675	0·4988
Zone 2: proportion of Q_s	0·6250	0·6780	0·6750	0·7082	0·8507
λ	−0·0471	−0·0540	−0·1084	−0·1342	−0·1868
r^2	0·4694	0·4868	0·4927	0·3323	0·2984

* Q_s is mass flux transported within 13 mm of the sand bed measured by optical sensor; $q_{(z)}$ is mass flux (g cm^{-2} s^{-1}) through 'pixel' height (*c.* 19 μm).

(typically 20 per cent) and probably arises from a grain population moving in energetic successive saltation. For moderate and fast wind speeds the rate of mass flux decay scales with the transport rate near the surface. The parameters α and λ in Equation 1 are unique for a sand of given textural characteristics but λ is well constrained in these data by the friction velocity (u_{*w}) calculated from the 'Law of the Wake' for wind speeds significantly greater than threshold. This finding suggests that a well defined relation may exist between λ and total mass flux.

- Below *c.*19 mm from the bed, mass flux decays much more rapidly as a power function of elevation. Mass flux at these elevations constitutes about 80 per cent of total transport but is underestimated by passive traps by about 37 per cent. This transport population most probably represents low-energy ejecta resulting from grain impacts.
- Below 2 mm from the bed, a sub-region of intense grain activity is observed which accounts for between 14 and 37 per cent of transport below 15 mm (11–30 per cent of total mass flux), depending on wind speed. An intermittent bed-contact transport population is inferred for this sub-region which diminishes significantly at fast wind speeds as transport in the region above is enhanced.
- Optical measurements of near-bed mass flux reveal structured patterns of locally high concentrations of mass flux in the lowest 5·5 mm above the bed. These show some velocity dependence, and probably represent dominant grain trajectory heights for the test sand. At fast wind speeds these patterns become less clear as grain motions become more varied and energetic.
- As grain trajectory heights scale approximately with u_*^2/g, profiles of horizontal mass flux are commonly related to the vertical scale height $\lambda zg/u_*^2$. However, the determination of friction velocity is problematic, especially in small wind tunnels. A more appropriate height scale would be $V_{ze}^2/2g$, where V_{ze} is the vertical component of grain ejection velocity.
- Mean velocity profiles measured during saltation in a wind tunnel boundary layer 0·17 m thick are shown to contain two clearly log-linear segments separated by a transitional region between 20 and 50 mm from the bed. Calculation of friction velocities conventionally from either segment does not yield appropriate

values. Application of a wake-correction effectively removes this pattern and provides usable values of friction velocity, u_{*w}. Near-bed mass flux measured by the optical sensor scales with u_{*w} 2·75.

- The observed kink in the fluid stress profile shows no clear relation to the measured mass flux gradients. If, as McEwan (1993) reasons, a kink exists due to a maximum in the force per unit volume exerted by the grains, then this may well relate more to the elevations of the high grain concentrations observed in these experiments at heights between 2 and 5·5 mm from the bed.
- Measurement of near-bed transport rates using simple, partially aspirated traps is unreliable, but at heights above 19 mm above the bed, trap efficiency is close to unity. Below this height the mass flux profile includes a separate, intense grain transport population. Unfortunately, in this region simple sand traps give both poor spatial resolution of the mass flux profile and distortion due to trap inefficiency.

High-resolution data from an optical mass flux sensor have revealed the complexity of near-bed mass flux profiles at elevations < 17 mm, as well as the detail lost in measurements using intrusive sand traps. Further high-resolution measurements of mass flux of this kind in the near-bed region are needed to resolve the effects of bed texture, and further research is required if discrepancies with model predictions are to be resolved. Also, field measurements at this scale are required to validate the three-segment model of vertical mass flux profiles.

ACKNOWLEDGEMENTS

The development of the optical mass flux sensor used in this research was funded by the Natural Environment Research Council under Grant No. GR3/8413. This financial support is gratefully acknowledged. I wish to thank especially my fellow investigators on this project, Drs Ian McEwan and Peter-Jost Spies (University of Aberdeen) for stimulating and fruitful collaboration. The help of Kevin Lee (Science Faculty Workshops) who constructed the mechanical components of the optical sensor, and Paul Guinnessy for assistance with its development and software is also gratefully acknowledged. I am also grateful to Drs Keld Rømer Rasmussen and John Stout for their careful and perceptive reviews of an earlier version of this paper. Responsibility for the contents of the paper rests, however, solely with the author.

REFERENCES

Anderson, R. S. 1986. 'Erosion profiles due to particles entrained by wind: application of an eolian sediment-transport model.' *Bulletin of the Geological Society of America*, **97**, 1270–1278.

Anderson, R. S. and Haff, P. K. 1988. 'Simulation of eolian saltation', *Science*, **241**, 820–823.

Anderson, R. S. and Haff, P. K. 1991. 'Wind modification and bed response during saltation of sand in air'. *Acta Mechanica*, Suppl. 1, 21–51.

Araoka, K. and Maeno, N. 1981. 'Dynamical behaviour of snow particles in the saltation layer', Proceedings of the Third Symposium on Polar Meteorology and Glaciology, National Institute of Polar Research, Tokyo, Technical Memorandum **19**, 253–263.

Arnold, S. A. 1998. Spatial and temporal development of saltation in air, PhD thesis, Geography Department, Queen Mary and Westfield College, University of London, 180 pp.

Bagnold, R. A. 1941. The Physics of Blown Sand and Desert Dunes, Methuen, London, 265 pp.

Butterfield, G. R. 1991. 'Grain transport rates in steady and unsteady turbulent airflows', *Acta Mechanica*, Suppl. 1, 97–122.

Butterfield, G. R. 1993. 'Sand transport response to fluctuating wind velocity', in Clifford, N. J., French, J. R. and Hardisty, J. (Eds) Turbulence: Perspectives on Flow and Sediment Transport, John Wiley and Sons, Chichester, 305–335.

Butterfield, G. R. 1998. 'Transitional behaviour of saltation: wind tunnel observations of unsteady winds', *Journal of Arid Environments*, **39**, 377–394.

Butterfield, G. R. 1999. 'Application of thermal anemometry and high-frequency measurement of mass flux to aeolian sediment transport research', *Geomorphology*, in press.

Chen, W., Yang, Z. and Dong, Z. 1996. 'Vertical distribution of wind-blown sand flux in the surface layer during sand storms in the Taklamakan Desert, Central Asia', *Physical Geography*, **17**, 193–218.

Coles, D. 1956. 'The law of the wake in the turbulent boundary layer', *Journal of Fluid Mechanics*, 1, 191–226.

Gerety, K. M. 1985. Problems with determination of U_* from wind-velocity profiles measured in experiments with saltation', in Barndorff-Neilsen, O. E. et al. (Eds), Proceedings of the International Workshop on the Physics of Blown Sand, Memoirs No. 8 Department of Theoretical Statistics, University of Aarhus, Denmark, vol. **2** 271–300.

Gillette, D. A. and Stockton, P. H. 1989. 'The effect of nonerodible particles on wind erosion of erodible surfaces', *Journal of Geophysical Research*, **94**(D10), 12885–12893.

Greeley, R., Blumberg, D. G. and Williams, S. H. 1996. 'Field measurements of the flux and speed of wind-blown sand', *Sedimentology*, **43**, 41–52.

Horikawa, K. and Shen, H. W. 1960. Sand movement by wind action (On the characteristics of sand traps), US Army Corps of Enginers, Beach Erosion Board, Technical Memorandum No. 119, 51 pp.
Irwin, H. P. A. P. H. 1981. 'The design of spires for wind simulation', *Journal of Wind Engineering and Industrial Aerodynamics*, **7**, 361–366.
Janin, L. F. and Cermak, J. E. 1988. 'Sediment-laden velocity profiles developed in a long boundary-layer wind tunnel', *Journal of Wind Engineering and Industrial Aerodynamics*, **28**, 159–168.
Jensen, J.L, Rasmussen, K. R., Sørensen, M. and Willetts, B. B. 1984. The Hanstholm experiment, 1982. Sand grain saltation on a beach, Department of Theoretical Statistics, Institute of Mathematics, University of Aarhus, Denmark, Research Report, No. 125.
Jones, J. R. and Willetts, B. B. 1979. 'Errors in measuring uniform aeolian sand flow by means of an adjustable trap', *Sedimentology*, **26**, 463–468.
Kawamura, R. 1951. Study on sand movement by wind, Report of the Physical Sciences Research Institute, University of Tokyo, 5, 95–112 (translated from Japanese by the National Aeronautic and Space Administration (NASA), Washington D.C., 1972).
Klebanoff, P. 1954. Characteristics of turbulence in a boundary layer with zero pressure gradient, National Advisory Committee on Aeronautics, Washington, Technical Note 3178.
McEwan, I. K. 1991. The Physics of Sand Transport by Wind, PhD Thesis, University of Aberdeen, 121 pp.
McEwan, I. K. 1993. 'Bagnold's kink: a physical feature of the wind velocity profile modified by blown sand', *Earth Surface Processes amd Landforms*, **18**, 145–156.
McEwan, I. K. and Willetts, B. B. 1991. 'Numerical model of the saltation cloud', *Acta Mechanica*, Suppl., 1, 53–66.
McEwan, I. K. and Willetts, B. B. 1993. 'Adaptation of the near-surface wind to the development of sand transport', *Journal of Fluid Mechanics*, **252**, 99–115.
McKenna Neuman, C. and Maljaars, M. 1997. 'Wind tunnel measurement of boundary-layer response to sediment transport', *Boundary-Layer Meteorology*, **84**, 67–83.
McKenna Neuman, C. and Nickling, W. G. 1994. 'Momentum extraction with saltation: implications for experimental evaluation of wind profile parameters', *Boundary-Layer Meteorology*, **68**, 35–50.
Nalpanis, P. 1985. 'Saltating and suspended particles over flat and sloping surfaces. II. Experiments and numerical simulations', in Barndorff-Neilsen, O. E. et al. (Eds), Proceedings of the International Workshop on the Physics of Blown Sand, Memoir No. 8, Department of Theoretical Statistics, University of Aarhus, Denmark, Vol. **1**, 37–66.
Nalpanis, P., Hunt, J. C. R. and Barrett, C. F. 1993. 'Saltating particles over flat beds.' *Journal of Fluid Mechanics*, **251**, 661–685.
Nickling, W. G. and McKenna Neuman, C. 1997. 'Wind tunnel evaluation of a wedgeshaped aeolian sediment trap', *Geomorphology*, **18**, 333–345.
Owen, P. R. 1964. 'Saltation of uniform grains in air', *Journal of Fluid Mechanics*, **20**, 225–242.
Owen, P. R. and Gillette, D. A. 1985. 'Wind tunnel constraint on saltation', in Barndorff-Neilsen, O. E. et al. (Eds), Proceedings of the International Workshop on the Physics of Blown Sand, Memoir No. 8, Department of Theoretical Statistics, University of Aarhus, Denmark, Vol. **2**, 253–269.
Rasmussen, K. R. and Mikkelsen, H. E. 1998. 'On the efficiency of vertical array aeolian field traps', *Sedimentology*, **45**, 789–800.
Rasmussen, K. R. and Sørensen, M. 1999. 'Initiation of aeolian mass transport in natural winds', *Earth Surface Processes and Landforms*, **24**, in press.
Rasmussen, K. R. Sørensen, M. and Willetts, B. B. 1985. 'Measurement of saltation wind strength on beaches', in Barndorff-Neilsen, O. E. et al. (Eds) Proceedings of the International Workshop on the Physics of Blown Sand Memoir No. 8, Department of Theoretical Statistics University of Aarhus, Denmark Vol. **2** 301–325.
Rasmussen, K. R., Iversen, J. D. and Rautahemio, P. 1996. 'Saltation and wind-flow interaction in a variable slope wind tunnel', *Geomorphology*, **17**, 19–28.
Rice, M. A., Willetts, B. B. and McEwan, I. K. 1995. 'An experimental study of multiple grain size ejecta produced by collisions of saltating grains with a flat bed', *Sedimentology*, **42**, 695–706.
Rice, M. A., Willetts, B. B. and McEwan, I. K. 1996. 'Observations of collision of saltating grains with a granular bed from high-speed cine-film', *Sedimentology*, **43**, 21–31.
Shao, Y., McTainsh, G. H. and Leys, J. F. 1993. 'Efficiencies of sediment samplers for wind erosion measurement', *Australian Journal of Soil Research*, **31**, 519–532.
Sørensen, M. 1985. 'Estimation of some aeolian sand transport parameters from transport rate profiles', in Barndorff-Neilsen, O. E. et al. (Eds), Proceedings of the International Workshop on the Physics of Blown Sand Memoir No. 8, Department of Theoretical Statistics, University of Aarhus, Denmark, Vol. **1**, 141–190.
Sørensen, M. 1991. 'An analytical model of wind-blown sand transport', *Acta Mechanica*, Suppl., 1, 67–81.
Spaan, W. P. and van den Abeele, G. D. 1991. 'Wind borne particle measurements with acoustic sensors', *Soil Technology*, **4**, 51–63.
Spies, P.-J. 1996. The Transport of Sand in Unsteady Winds, PhD thesis, University of Aberdeen, 93 pp.
Spies, P.-J. and McEwan, I. K. 1999a. 'One-dimensional transition behaviour in saltation', *Earth Surface Processes and Landforms*, (in press.)
Spies, P.-J. and McEwan, I. K. 1999b. 'Equilibration of saltation', *Earth Surface Processes and Landforms*, (in press).
Spies, P.-J., McEwan, I. K. and Butterfield, G. R. 1995. 'On wind velocity profile measurements taken in wind tunnels with saltating grains', *Sedimentology*, **42**, 515–521.
Sterk, G. and Raats, P. A. C. 1996. 'Comparison of models describing the vertical distribution of wind-eroded sediment', *Journal, Soil Science Society of America*, **60**, 1914–1919.
Stockton, P. and Gillette, D. A. 1990. 'Field measurement of the sheltering effect of vegetation on erodible land surfaces', *Land Degradation and Rehabilitation*, **2**, 77–85.
Stout, J. E. and Zobeck, T. M. 1996. 'The Wolfforth Field Experiment: a wind erosion study', *Soil Science*, **161**, 616–632.
Ungar, J. E. and Haff, P. K. 1987. 'Steady state saltation in air', *Sedimentology*, **34**, 289–299.
Werner, B. 1990. 'A steady state model of wind-blown sand transport', *Journal of Geology*, **98**, 1–17.
White, B. R. 1982. 'Two-phase measurements of saltating boundary layer flow', *International Journal of Multiphase Flow*, 5, 459–473.

White, B. R. and Mounla, H. 1991. 'An experimental study of Froude number effect on wind-tunnel saltation', *Acta Mechanica*, Suppl. 1, 145–157.
White, B. R. and Schultz, J. C. 1977. 'Magnus effect in saltation', *Journal of Fluid Mechanics*, **81**, 497–512.
White, F. M. 1991. Viscous Fluid Flow, McGraw-hill, New York, 611 pp.
Willetts, B. B. and Rice, M. A. 1985. 'Inter-saltation collisions', in Barndorff-Neilsen, O. E. et al. (Eds), Proceedings of the International Workshop on the Physics of Blown Sand, Memoir No. 8, Department of Theoretical Statistics, University of Aarhus, Denmark, Vol. **1** 83–100.
Willetts, B. B. and Rice, M. A. 1986. 'Collision in aeolian transport: the saltation/creep link', in Nickling, W. G. (Ed.), Aeolian Geomorphology, Proceedings of the 17th Annual Binghamton Geomorphology Symposium, Guelph, Ontario, Canada, Allen and Unwin, Boston, 1–17.
Williams, G. 1964. 'Some aspects of aeolian saltation load', *Sedimentology*, **3**, 257–287.
Zingg, A. W. 1953. 'Wind tunnel studies of the movement of sedimentary material', Proceedings of the Fifth Hydraulic Conference, Iowa University Studies in Engineering Bulletin, 34, 111–135.

